

Stability of traveling, pre-tensioned, heavy cables

Abhinav R. Dehadrai*, Ishan Sharma, and Shakti S. Gupta

Mechanics & Applied Mathematics Group, Department of Mechanical Engineering, Indian Institute of Technology Kanpur, Kanpur 208016, India

Abstract

We study the dynamics of an inclined tensioned, heavy cable traveling with a constant speed in the vertical plane. The cable is modeled as a beam resisting bending and shear. The governing equation for the transverse in-plane vibrations of the cable are derived through the Newton-Euler method. The cable dynamics is also studied in the limit of zero bending stiffness. In all cases, application of energy balance reveals that the total energy of the system fluctuates even though the oscillations are small and bounded in time, indicating that the system is nonconservative. A comprehensive stability analysis is carried out in the parameter space of inclination, traveling speed, pre-tension, bending rigidity and the slenderness of the cable. Effect of damping is also considered. We conclude that, while pre-tension, rigidity and slenderness enhance the stability of the traveling cable, the angle of inclination affects the stability adversely. These results may act as guidelines for safer design and operation.

Keywords: Traveling cables; Stability; Vibrations

1 Introduction

Traveling cables are fundamental driving mechanisms in elevators, conveyor belts, automobile chain-drives, cableways, etc. In these, all or part of the cable is inclined to gravity. During operations the cable tends to oscillate transversely as it travels longitudinally (Sack, 1954), (Miranker, 1960), (Swope and Ames, 1963), (Mote, 1965), (Mote, 1966), (Barakat, 1968), (Thurman and Mote, 1969), (Rogge, 1972), (Wickert and Mote, 1989), (Wickert and Mote, 1990), (Wickert, 1992). To prevent breakdown due to fatigue these oscillations need to remain within some design limits. In these studies, cables are modeled either as an elastic beam that resists bending moment and shear, or as a string which supports no bending or shear.

The dynamics of *horizontally* traveling (traveling direction normal to gravity) beams and strings is well studied (Sack, 1954), (Miranker, 1960), (Swope and Ames, 1963), (Mote, 1965), (Mote, 1966), (Barakat, 1968), (Thurman and Mote, 1969), (Rogge, 1972), (Wickert and Mote, 1989), (Wickert and Mote, 1990), (Wickert, 1992). Most work has focused on modal analysis to obtain natural frequencies (eigenvalues) at different operating speeds. Eigenvalues appear as complex conjugates, in which the imaginary part

*Email: abhinavd@iitk.ac.in

contributes to oscillations while the real part controls the amplitude. During stable operations the real part is absent. Therefore, the *critical speed* at which the eigenvalue first appears as a conjugate pair is of special interest. At this speed the amplitude may grow with time by virtue of the positive real part, leading to instability. In the case of horizontally traveling strings, (Miranker, 1960) investigated the continuous energy influx from the material outside the boundary. Response to harmonic support excitation was also studied in (Miranker, 1960), and the instability was identified with the resonance frequency, as the amplitude of the vibration grew with time. Discussions on dissipation and stability of general dynamical systems are found in (Ziegler, 2013).

The critical speed of a traveling cable varies with the type of supports and the distance between them. The arc-length based model of a spatially traveling string proposed by (Rogge, 1972) generalized all its preceding models, and the static equilibrium equation of a string supported at its ends (Aleksiev, 1964) was obtained as a special case. The calculations in (Barakat, 1968) of the energy flow in a dissipation-free model were later improved when an additional energy influx from the supports was identified by (Wickert and Mote, 1989). However, it was noted that the total energy during steady horizontal travel was not constant in spite of zero damping. Thus, the system was nonconservative whether or not the modal analysis predicted instability.

Most results on horizontally traveling beams and strings have been compiled by (Hagedorn and DasGupta, 2007) and (Banichuk et al., 2013). They include discussions on modal, transient and energy analyses. We restrict ourselves from visiting them individually, due to constraint of space, and focus primarily on cables traveling in a vertical plane inclined to gravity. By virtue of this inclination a portion of the cable's weight is distributed along its length. This, in turn, affects the critical speed at which instability sets in. To the best of our knowledge this case has not yet been investigated.

The paper is organized as follows. We begin by modeling the cable as a beam that resists bending and shear, and which travels at an inclination, while resting upon small rollers; see Fig. 1. A string model, useful for very flexible cables, is obtained as a special case. We then perform a modal analysis to identify the relation between speed, inclination, tension, bending rigidity, slenderness ratio and the conditions of instability. Finally, we verify the instability from evolution of both the energy and the amplitude of oscillations obtained after direct time-integration of the model. The concluding section summarizes the implications on cable design of our analyses.

2 Governing equations

A heavy cable traveling between two pairs of small rollers is shown in Fig. 1. The cable is inclined at an angle φ from the horizontal. The plane is defined using the fixed coordinate system X - Y , which is aligned with the cable, and has its origin in between the bottom rollers. The distance between the top and bottom rollers is L and the acceleration due to gravity g acts vertically downwards. The cable has uniform mass density ρ , cross-section A_c , Young's modulus E , and cross-sectional area moment of inertia I . The speed v of each material particle along the length of the cable is constant. The displacement $y = y(x, t)$ along the transverse (Y -axis) of a material point located at x is measured from its static equilibrium $y_{st}(x)$. Both y and y_{st} are assumed to be small.

Employing the notation $\partial_x^n = (\partial^n / \partial x^n)$ and $\partial_t^n = (\partial^n / \partial t^n)$ for the n^{th} order partial

derivatives with respect to x and t , respectively, the total transverse velocity is

$$\dot{y} = \frac{dy}{dt} = \partial_t y + v \partial_x y,$$

where $\partial_t y$ is called the *local* velocity and $v \partial_x y$ is the *convective* velocity of a material point. The total acceleration is

$$\ddot{y} = \frac{d\dot{y}}{dt} = \partial_t^2 y + 2v \partial_x \partial_t y + v^2 \partial_x^2 y,$$

where $\partial_t^2 y$ is the *local* acceleration, $2v \partial_x \partial_t y$ is a gyroscopic term and $v^2 \partial_x^2 y$ is the convective acceleration.

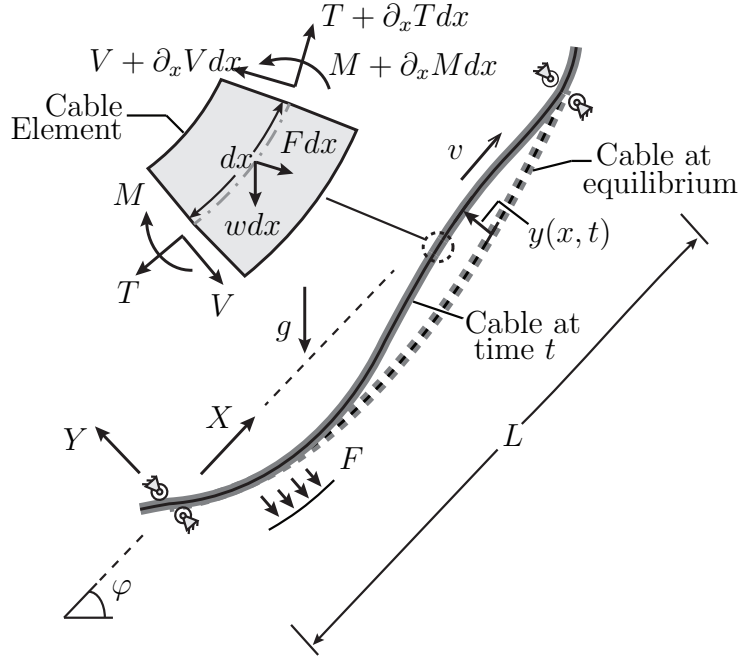


Figure 1: Schematic of a traveling cable at time t (solid curve) and at its static equilibrium (broken curve). The free-body diagram of a material element is also shown. The deflections of the cable are exaggerated for clarity.

The free body diagram of an infinitesimal cable element with length dx and weight per unit length $w = \rho A_c g$ is also shown in Fig. 1. To account for possible presence of fluid drag, a transversely distributed loading $F(x, t) = \zeta \dot{y}$, with damping coefficient ζ , is applied on the element. The balance of angular momentum about the centroid of the element yields the shear force

$$V = \partial_x(\rho I \ddot{y} - M),$$

where $M = EI \partial_x^2 y$ is the bending moment. For small transverse deflection, the weight of the cable causes its tension to vary along the cable's length:

$$T(x) = T(L) - (L - x) w \sin \varphi,$$

where we assume that the tension $T(L)$ at $x = L$ is known. The linear momentum balance in longitudinal and transverse directions shows that the equilibrium deflection of the beam

is governed by

$$[EI\partial_x^4 - \partial_x\{T(x) \partial_x\}]y_{\text{st}} + w \cos \varphi = 0 \quad (1a)$$

$$\text{with } y_{\text{st}}(0) = y_{\text{st}}(L) = \partial_x^2 y_{\text{st}}(0) = \partial_x^2 y_{\text{st}}(L) = 0. \quad (1b)$$

Similarly, the transverse vibrations of the beam about the equilibrium are governed by

$$[EI\partial_x^4 - \partial_x\{T(x) \partial_x\}]y + \zeta \dot{y} + (\rho A_c - \rho I \partial_x^2) \ddot{y} = 0 \quad (2a)$$

$$\text{with } y(0, t) = y(L, t) = \partial_x^2 y(0, t) = \partial_x^2 y(L, t) = 0. \quad (2b)$$

In (2), the term $EI\partial_x^4 y$ accounts for bending rigidity, while $\rho I \partial_x^2 \ddot{y}$ is the rotary inertia. When $\varphi = 0$, we recover transverse vibrations of a horizontally traveling Rayleigh beam, while the Euler-Bernoulli beam of (Hagedorn and DasGupta, 2007) is recovered when rotary inertia is also ignored.

2.1 Special case: string model

For a heavy cable which is highly flexible and has negligible shear and bending stiffness, a simple model, resembling the conventional string model, is arrived at by ignoring EI in (1) and (2). This yields the governing equation for the equilibrium state:

$$[-\partial_x\{T(x) \partial_x\}]y_{\text{st}} + w \cos \varphi = 0 \quad (3a)$$

$$\text{with } y_{\text{st}}(0) = y_{\text{st}}(L) = 0, \quad (3b)$$

while transverse vibrations are governed by

$$[-\partial_x\{T(x) \partial_x\}]y + \zeta \dot{y} + \rho A_c \ddot{y} = 0 \quad (4a)$$

$$\text{with } y(0, t) = y(L, t) = 0. \quad (4b)$$

The equation for a horizontally traveling string considered in (Hagedorn and DasGupta, 2007) is retrieved from (4) by setting $\varphi = 0$.

2.2 Nondimensionalization

For further analysis, the dimensionless forms of the governing equations (1) and (2) are derived here. To this end, we introduce nondimensional quantities

$$\bar{x} = x/L, \bar{y} = y/L, \bar{t} = t(EI/\rho A_c L^4)^{1/2}, \bar{v} = v(EI/\rho A_c L^2)^{-1/2}, \\ \mu = \{T(L)L^2/EI\}^{1/2}, \varrho = wL^3/EI, \lambda = (I/L^2 A_c)^{-1/2} \text{ and } c = \zeta(EI\rho A_c/L^2)^{-1/2}.$$

The dimensionless end tension μ will be employed as a control parameter to vary tension in the cable. With these (1) becomes

$$[\bar{\partial}_x^4 - \bar{\partial}_x\{\bar{T}(\bar{x}) \bar{\partial}_x\}]\bar{y}_{\text{st}} + \varrho \cos \varphi = 0 \quad (5a)$$

$$\text{and } \bar{y}_{\text{st}}(0) = \bar{y}_{\text{st}}(1) = \bar{\partial}_x^2 \bar{y}_{\text{st}}(0) = \bar{\partial}_x^2 \bar{y}_{\text{st}}(1) = 0, \quad (5b)$$

while (2) transforms to

$$[\bar{\partial}_x^4 - \bar{\partial}_x\{\bar{T}(\bar{x}) \bar{\partial}_x\}]\bar{y} + c \dot{\bar{y}} + (1 - \lambda^{-2} \bar{\partial}_x^2) \ddot{\bar{y}} = 0 \quad (6a)$$

$$\text{and } \bar{y}(0, \bar{t}) = \bar{y}(1, \bar{t}) = \bar{\partial}_x^2 \bar{y}(0, \bar{t}) = \bar{\partial}_x^2 \bar{y}(1, \bar{t}) = 0, \quad (6b)$$

where $\bar{\partial}_x = \partial/\partial\bar{x}$ and $\bar{\partial}_t = \partial/\partial\bar{t}$, and the nondimensional tension

$$\bar{T}(\bar{x}) = \mu^2 - (1 - \bar{x}) \varrho \sin \varphi. \quad (7)$$

For the string of Sec. 2.1 we employ the following nondimensionalization:

$$\begin{aligned} \bar{x} &= x/L, \bar{y} = y/L, \bar{t} = t \{T(L)/\rho A_c L^2\}^{1/2}, \bar{v} = v \{T(L)/\rho A_c\}^{-1/2}, \\ \varrho &= wL/T(L), \bar{T}(\bar{x}) = T(x)/T(L) \text{ and } c = \zeta L \{T(L)/\rho A_c\}^{1/2} \end{aligned}$$

With these (3) becomes

$$[-\bar{\partial}_x \{\bar{T}(\bar{x}) \bar{\partial}_x\}] \bar{y}_{\text{st}} + \varrho \cos \varphi = 0, \quad (8a)$$

and

$$\bar{y}_{\text{st}}(0) = \bar{y}_{\text{st}}(1) = 0, \quad (8b)$$

while (4) becomes

$$[-\bar{\partial}_x \{\bar{T}(\bar{x}) \bar{\partial}_x\}] \bar{y} + c \dot{\bar{y}} + \ddot{\bar{y}} = 0, \quad (9a)$$

and

$$\bar{y}(0, \bar{t}) = \bar{y}(1, \bar{t}) = 0. \quad (9b)$$

We now solve for the equilibrium shapes before proceeding to the dynamics of cables.

3 Equilibrium shapes

The equilibrium shape of an inclined, heavy beam is found by solving (5) numerically. The computational algorithm is explained in the next section. The equilibrium shape of a heavy, inclined string, on the other hand, is found from (8) in closed form:

$$\bar{y}_{\text{st}}(\bar{x}) = -\cot \varphi \{G(\bar{x}) - \bar{x}\}$$

where

$$G(\bar{x}) = \frac{\log |\bar{T}(\bar{x})/\bar{T}(0)|}{\log |\bar{T}(1)/\bar{T}(0)|}$$

is the percentage gain in tension at location x along the cable's length relative to the tension at the top end. When $\varphi = \pi/2$ the string hangs vertically down, while for the horizontal string ($\varphi = 0$) the static equilibrium shape $\bar{y}_{\text{st}} = \varrho(\bar{x}^2 - \bar{x})/2$ is a parabola¹. The equilibrium shapes of strings and beams at various inclinations and end-tensions are shown in Fig. 2.

We find from Fig. 2 that lower the inclination, closer is the equilibrium shape to a parabola, and lesser is the lengthwise gain in tension. In the inset we compare the string's equilibrium shape with that of a beam, which carries the same tension $\bar{T}(\bar{x}) = 1 - (1 - \bar{x}) \sin \varphi$ as that of the string. As expected, the string sags more than the beam due to the absence of bending rigidity. Finally, the beam bends less with increase in tension.

We next describe the numerical techniques employed for the modal, transient and energy analyses.

¹In general, a simply supported string deforms to the classical catenary (*cosh*) curve under the action of its own weight. However, when the displacement is small, as assumed in Sec. 2, this curve becomes a parabola.

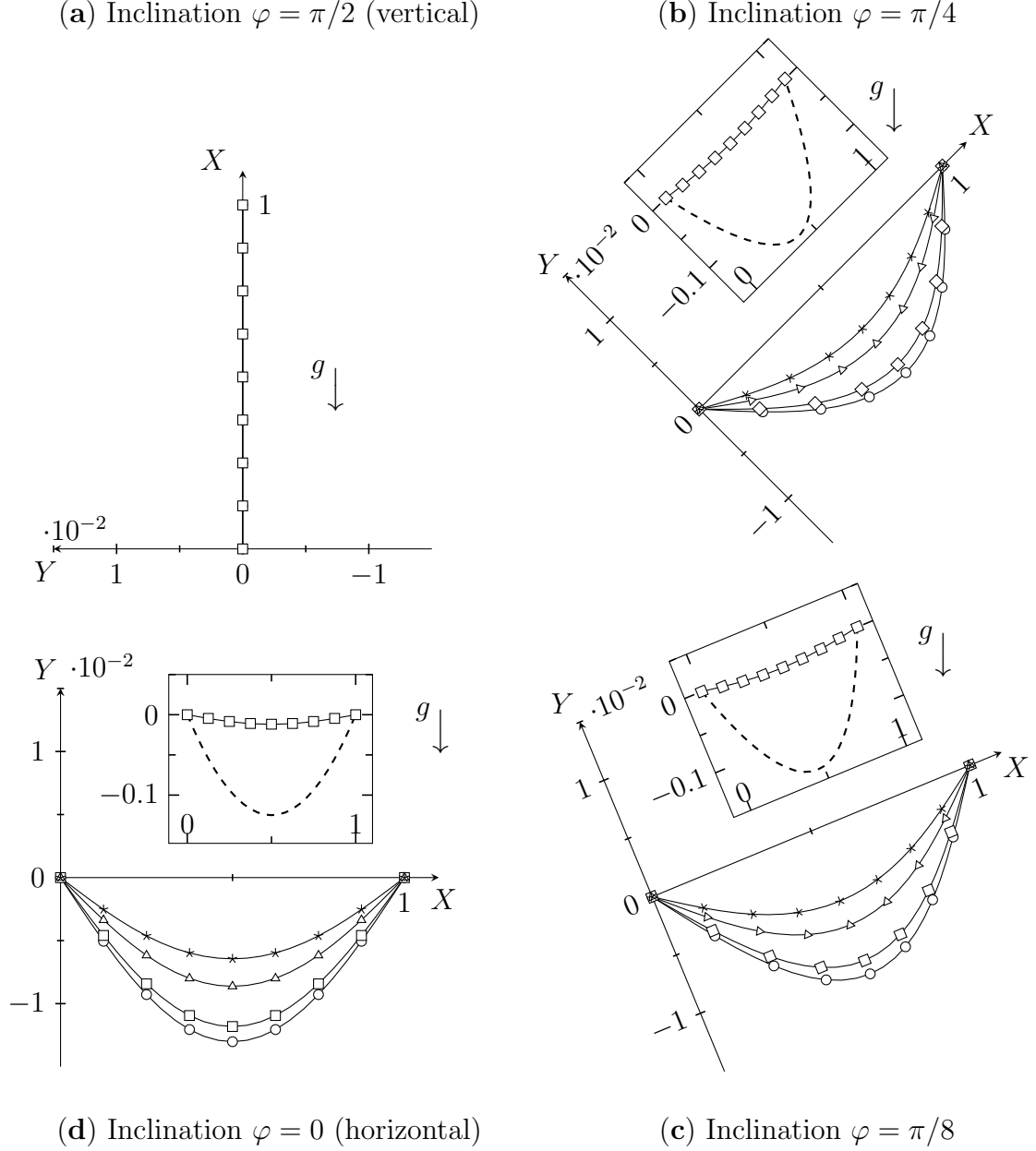


Figure 2: Equilibrium shapes of beams at several inclinations φ held by various dimensionless tensions: $\mu = 0$ ($-\circ-$), $\mu = 1$ ($-\square-$), $\mu = 5$ ($-\triangle-$) and $\mu = 10$ ($-\ast-$). The equilibrium shapes of a string ($- - -$) and a beam ($-\square-$) with tension $\mu = 1$ are compared in the insets. The dimensionless mass per unit length $\varrho = 1$.

4 Numerical solution

The governing equations (2) and (4), or their dimensionless forms (6) and (9), are not self-adjoint. The Galerkin method (Meirovitch and Hagedorn, 1994) is reliable for numerically solving such problems. It is now described.

Assume the expansion

$$\bar{y}_N(\bar{x}, t) = \mathbf{s}^T \mathbf{b}, \quad (10)$$

where $\mathbf{s}(\bar{x}) = [\sin(n\pi\bar{x})]^T$, for $n = 1 \dots N$, is an N -dimensional column vector of Fourier

sine modes, and $\mathbf{b}(\bar{t}) = [b_1(\bar{t}), b_2(\bar{t}), \dots, b_N(\bar{t})]^T$ is a column vector of time-varying unknown coefficients. The modes individually vanish at the boundaries, thereby satisfying the geometric boundary conditions. Then (6) evaluated at $\bar{y} = \bar{y}_N$ results in an error, called the *residue*. By setting the projections of the residue on the N Fourier sine modes to zero yields a set of N differential algebraic equation, which may be cast in the following state-space form:

$$\frac{d\mathbf{q}}{d\bar{t}} = \mathbf{A}\mathbf{q}, \quad (11a)$$

where the state vector and the state matrix are, respectively,

$$\mathbf{q} = \begin{bmatrix} \dot{\mathbf{b}} \\ \mathbf{b} \end{bmatrix} \quad \text{and} \quad \mathbf{A} = \int_0^1 \begin{bmatrix} -\mathbf{M}^{-1}\mathbf{C} & \mathbf{1} \\ -\mathbf{M}^{-1}\mathbf{K} & \mathbf{0} \end{bmatrix} d\bar{x}, \quad (11b)$$

with $\mathbf{1}$ representing an $N \times N$ identity matrix and $\mathbf{0}$ being the $N \times N$ zero matrix, while

$$\mathbf{M} = (\mathbf{s}\mathbf{s}^T) - \lambda^{-2} (\mathbf{s}'\mathbf{s}'^T), \quad \mathbf{C} = c \{\mathbf{s}\mathbf{s}^T\} + 2\bar{v} (\mathbf{s}\mathbf{s}'^T + \lambda\mathbf{s}'\mathbf{s}''^T) \quad (12a, b)$$

and

$$\mathbf{K} = (1 - \lambda^{-2}\bar{v}^2) (\mathbf{s}''\mathbf{s}''^T) + (\bar{v}^2 - \bar{T}(\bar{x})) (\mathbf{s}'\mathbf{s}'^T) + \frac{c\bar{v}}{2} (\mathbf{s}\mathbf{s}'^T - \mathbf{s}'\mathbf{s}^T) \quad (12c)$$

are the mass, damping and stiffness matrices, respectively, with the $()'$ denoting $d/d\bar{x}$. Note that the mass matrix \mathbf{M} is symmetric, while the damping matrix \mathbf{C} has a symmetric part $c(\mathbf{s}\mathbf{s}^T)$ and a skew-symmetric part $2\bar{v}(\mathbf{s}\mathbf{s}'^T + \lambda\mathbf{s}'\mathbf{s}''^T)$ called the gyroscopic damping. From the stiffness matrix \mathbf{K} , after replacing for \bar{T} from (7), we obtain four terms: the material stiffness $(1 - \lambda^{-2}\bar{v}^2) (\mathbf{s}''\mathbf{s}''^T)$, the geometric stiffness $(\bar{v}^2 - \mu^2) (\mathbf{s}'\mathbf{s}'^T)$, the stiffness $\varrho \cos \varphi (1 - \bar{x}) (\mathbf{s}'\mathbf{s}'^T)$ due to the cable's weight, and the stiffness $c\bar{v} (\mathbf{s}\mathbf{s}'^T - \mathbf{s}'\mathbf{s}^T)/2$ due to damping. While the first three stiffness terms are symmetric, the last one is skew-symmetric. The state-space form for the string model (9) may be obtained by setting $\lambda^{-2} = 0$ and $\mu = 1$ in (12).

Equation (11) may be treated as an *eigenvalue* problem for *modal analysis*, or an initial value problem for *transient analysis*. In modal analysis, the cable's natural frequencies corresponding to the specified modes are extracted directly from (11). They provide a qualitative insight into the system (Ziegler, 2013). In a transient analysis the solution $\mathbf{b}(\bar{t})$ is calculated through direct time-integration of the state-space equation (11a) with given initial conditions $\mathbf{b}(0)$ and $\dot{\mathbf{b}}(0)$. The material displacements are then obtained from (10).

We now discuss modal analysis in detail, followed by a brief discussion of transient analysis.

4.1 Modal Analysis

An eigenvalue problem is formulated from (6) by setting $\mathbf{b}(\bar{t}) = [\exp(\omega_n \bar{t})]^T$, where ω_n is the eigenvalue (frequency) associated with the n^{th} mode, assumed to be given by $\sin(n\pi\bar{x})$. The state matrix \mathbf{A} in (11b) is *not* symmetric in general, but it has complex conjugate eigenvalues. Accordingly, the transverse displacement is

$$\bar{y}_N(\bar{x}, \bar{t}) = \text{Re} \sum_{n=1}^N \exp[\{\text{Re}(\omega_n) \pm i \text{Im}(\omega_n)\}\bar{t}] \sin(n\pi\bar{x}), \quad (13)$$

in which the N sinusoidal modes collectively define the instantaneous shape of the cable, while the oscillatory part $\exp\{\pm i \text{Im}(\omega_n)\bar{t}\}$ modulates the material point's vibration about its equilibrium state. The growth or decay of the amplitude of these vibrations is governed by $\exp\{\text{Re}(\omega_n)\bar{t}\}$. The real part of the eigenvalue, thus, governs the solution's, and hence the cable's instability. The eigenvalues depend upon the geometric and material parameters of the cable, *viz.* travel speed and inclination of the cable, tension and bending rigidity of the cable, and the cable's slenderness ratio.

The accuracy of modal analysis depends on the number of modes we consider for approximating the solution, and A discusses this.

4.2 Stability

Instability in operation corresponds to positive real part of the smallest eigenvalue. When

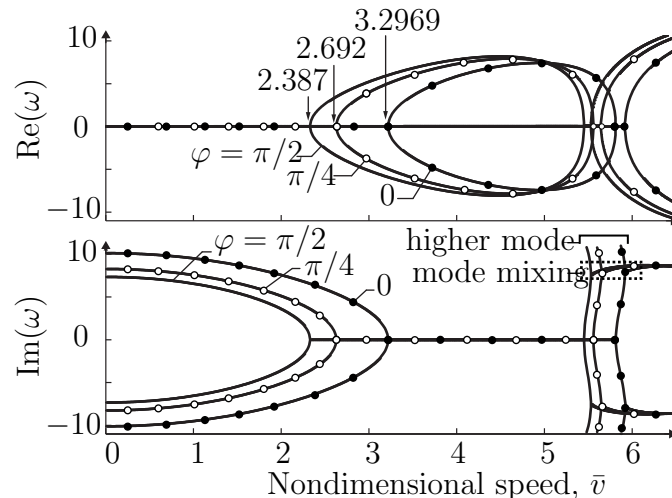


Figure 3: Comparison of the first eigenvalues for a cable modeled as a traveling Euler-Bernoulli beam, inclined at various angles to gravity: $\varphi = \pi/2$ represents the vertically traveling cable and $\varphi = 0$ is the horizontally traveling cable. The higher modes appear at later speeds and are observed to mix with the primary modes.

this happens the displacements grow exponentially with time. This may result in failure and/or bring in nonlinear effects, hitherto ignored. The instability criterion identifies the *critical value* of the governing parameter at which the real part of the smallest (first) eigenvalue first becomes positive. For example, in Fig. 3, from the bifurcation in $\text{Re}(\omega)$ we identify nondimensional speeds $\bar{v} = 2.387$, 2.692 and 3.2969 as the *critical* speeds for cables traveling at inclinations $\varphi = \pi/2, \pi/4$ and 0 , respectively. Beyond these critical speeds $\text{Re}(\omega)$ splits into a positive and a negative part, whereas $\text{Im}(\omega)$ vanishes. With increase in inclination the bifurcation point shifts to the left. This implies a lowering of the critical speed of operation with increasing inclination leading to an earlier onset of instability. The critical speed $\bar{v} = 3.2969$ for the horizontally traveling beam ($\varphi = 0$) agrees well with the value reported in (Wickert and Mote, 1990).

A higher tension in the cable stabilizes the system. This role of tension in enhancing stability is lowered by the action of gravity in inclined cables. This is illustrated in Fig. 4 that plots critical travel speed as a function of the dimensionless end tension μ for various inclinations φ . The resulting curve for a given φ is the boundary separating regions of stable and unstable operations, which lie below and above the curve, respectively. Stability

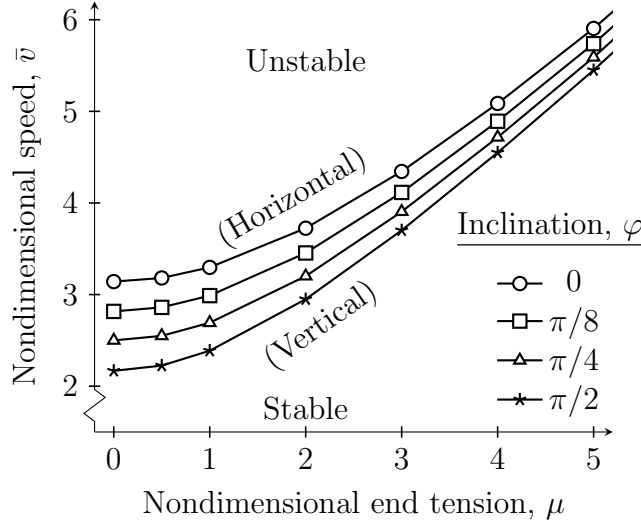


Figure 4: Stability curves for traveling Euler-Bernoulli beams at various inclinations φ are obtained by plotting the nondimensional speed \bar{v} as a function of nondimensional end tension μ . The parameter $\rho = 10$.

curves at intermediate values of inclination lie between those belonging to vertically and horizontally traveling cables. Furthermore, we observe that, as expected, increasing the cable tension delays the onset of instability, thereby ensuring stable operation at relatively higher speeds. Finally, we see that a more inclined cable becomes unstable at lower speeds. The preceding discussion is illustrated by the following example.

Example 1 A 0.5 mm diameter steel cable ($E = 210$ GPa, $\rho = 7800$ Kg/m³), traveling horizontally ($\varphi = 0$) between rollers which are $L = 1$ m apart, is stable when the end tension $T(L)$ is 1.75 mN ($\mu = 1$) and the speed is about 3.26 m/s ($\bar{v} = 3.29$); cf. Fig. 4. However, an inclined cable ($\varphi > 0$) under the same $T(L)$ is unstable at that speed. It becomes stable at lesser speeds: 2.95 m/s ($\bar{v} = 2.98$) when $\varphi = \pi/8$, 2.66 m/s ($\bar{v} = 2.69$) when $\varphi = \pi/4$ and 2.35 m/s ($\bar{v} = 2.38$) when traveling vertically ($\varphi = \pi/2$). Thus, inclination has a destabilizing effect.

Increasing the tension to $T(1\text{m}) = 7$ mN ($\mu = 2$) increases the critical speeds considerably: 3.68 m/s at $\varphi = 0$, 3.42 m/s at $\varphi = \pi/8$, 3.17 m/s at $\varphi = \pi/4$ and 2.92 m/s at $\varphi = \pi/2$. However, with further increase in tension to $T(1\text{m}) = 28$ mN ($\mu = 4$) the respective critical speeds: 5.04 m/s at $\varphi = 0$, 4.84 m/s at $\varphi = \pi/8$, 4.67 m/s at $\varphi = \pi/4$ and 4.50 m/s at $\varphi = \pi/2$, are closer to each other. The critical speeds for all φ converge while rising further; see Fig. 4. Thus, tension contributes to the stability.

Consider now a cable modeled as a Rayleigh beam wherein rotary inertia is retained. In a horizontally traveling Rayleigh beam the slenderness ratio λ improves the stability for any nonzero end-tension μ and mass density ρ , as shown by the solid curve in Fig. 5. At higher λ the rotary inertia term in (6) becomes small compared to the bending rigidity. Therefore, with increasing slenderness ratio, the stability boundary of the Rayleigh beam approaches that of a traveling Euler-Bernoulli beam (dashed line); the latter, of course, remains unaffected by the beam's slenderness when $\varphi = 0$.

In passing, we note from Fig. 6 that more inclined ($\varphi > 0$) traveling Euler-Bernoulli

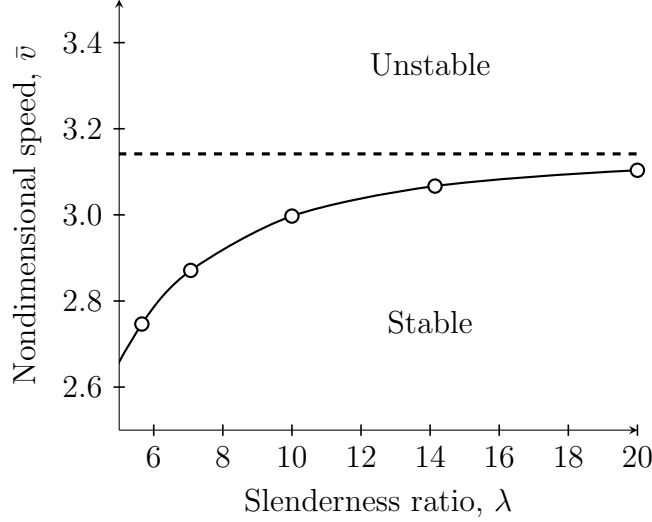


Figure 5: Stability curves obtained by plotting nondimensional speed \bar{v} as a function of slenderness ratio λ for horizontally traveling ($\varphi = 0$) Rayleigh (solid line) and Euler-Bernoulli (dashed line) beams.

beams with higher λ are slightly less stable than the horizontal ones. However, when λ is small, the inclination barely affects the Euler-Bernoulli beam's stability.

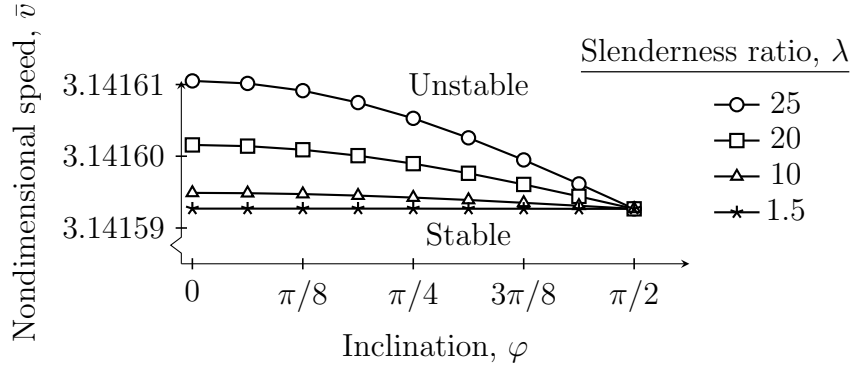


Figure 6: Variation with inclination φ of critical nondimensional speed \bar{v}_{crit} for cables modeled as Euler-Bernoulli beams. Several slenderness ratios λ are considered. Slender cables are slightly more stable for all non-zero inclinations.

Surprisingly, we find that an inclined ($\varphi > 0$) traveling Rayleigh beam is inherently unstable, i.e. at any $\varphi > 0$ the real part of the smallest eigenvalue is always positive, as shown in the inset of Fig. 7 for the case when $\varphi = \pi/4$. Moreover, unlike an Euler-Bernoulli beam (Fig. 3), the critical speed is different from the bifurcation speed $\bar{v}_{bif} = 2.671$ at which the smallest $\text{Re}(\omega)$ bifurcates and the associated $\text{Im}(\omega)$ vanishes.

However, we observe that the inclusion of damping ($c > 0$) shifts the real part of the first eigenvalue below zero, thereby removing the inherent instability of a traveling Rayleigh beam. The amount that $\text{Re}(\omega)$ shifts depends upon the amount of damping c introduced. For example, when $c = 5$ (Fig. 8) we identify $\bar{v}_{crit} = 2.692$ as the critical speed at which a real part of the smallest eigenvalues first begins to appear positive. More

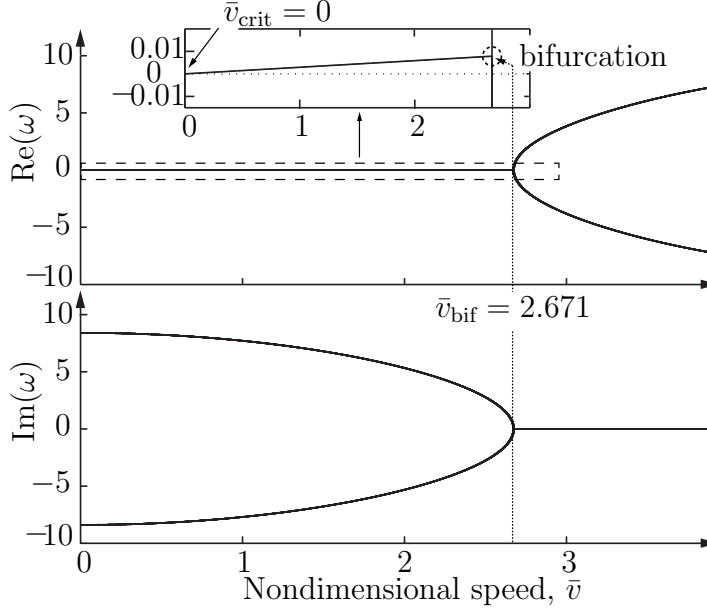


Figure 7: Real and imaginary part of the smallest (first) eigenvalue of an undamped ($c = 0$), inclined ($\varphi = \pi/4$), traveling Rayleigh beam are plotted as functions of speed. Other parameters are $\varrho = 10$, $\mu = 1$ and $\lambda = 5$. The inset shows the existence of positive real part at all nondimensional speeds $\bar{v} > 0$, while the bifurcation (as in Fig. 3) happens much later when $\bar{v} = \bar{v}_{\text{bif}} = 2.671$.

damping shifts \bar{v}_{crit} further to the right. This shift in critical speed due to damping may be employed to provide a suitable range of speeds $\bar{v} < \bar{v}_{\text{crit}}$ for stable operation. However, in the damped traveling Rayleigh beams of Fig. 8 the speed \bar{v}_{bif} at which the first eigenvalue bifurcates is less than \bar{v}_{crit} . This indicates the existence of complex eigenvalues at sub-bifurcation speeds, resulting in underdamped oscillations of the beam in its first mode during stable operation. We note that, in contrast to \bar{v}_{crit} , the bifurcation point in the damped beam shifts left, i.e. \bar{v}_{bif} decreases with increase in damping. We note from this behaviour of \bar{v}_{bif} that when c is increased enough, at a given \bar{v} eventually Im(ω) of the first mode will cease to appear. When this happens, the higher modes (not shown), similar to those found in Euler-Bernoulli beams (Fig. 3), become significant and govern the beam's oscillations.

Finally, we note that a damped Euler-Bernoulli beam shows a similar behaviour.

String model

For highly flexible cables (negligible bending rigidity), the tension in the cable and its inclination govern stability. Figure 9(a) plots travel speed \bar{v} as a function of inclination φ . The resulting stability curves correspond to different values of the scaled end tension

$$\mu_s = \frac{T(L)|_{\varphi}}{T(L)|_0},$$

which is a ratio of end tension $T(L)$ at inclination φ to that at $\varphi = 0$ (horizontal). We again note that less inclined cables are more unstable, and tension enhances stability. However, unlike for beams, the tension does *not* affect the critical speed of horizontally

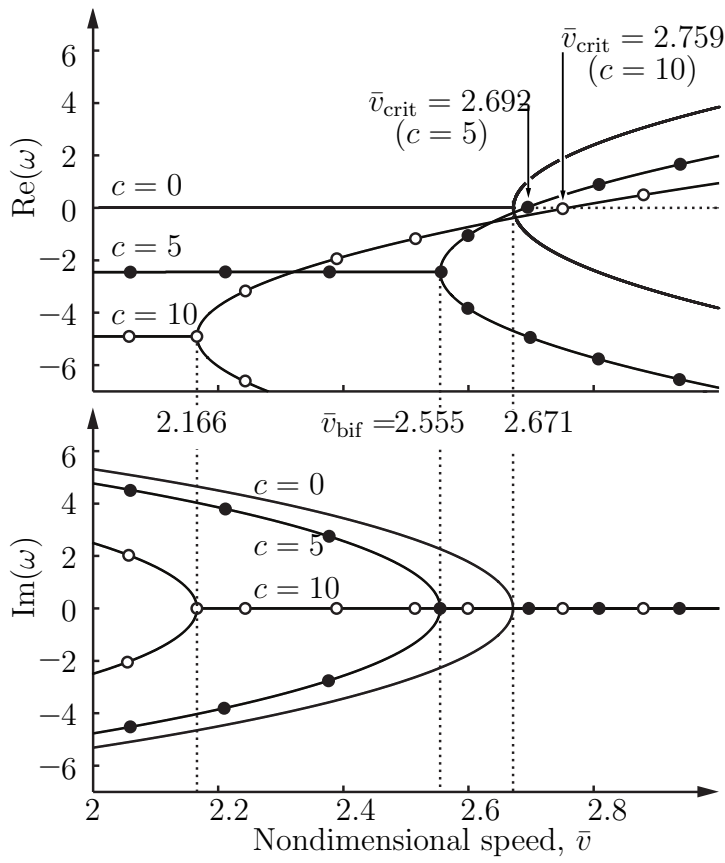


Figure 8: Real and imaginary parts of the first mode's eigenvalue ω for a damped, traveling Rayleigh beam are shown as functions of nondimensional speed \bar{v} for these values of nondimensional viscosity: $c = 0, 5$ and 10 . We observe that with damping the critical speed \bar{v}_{crit} increases from 0 for $c = 0$ to 2.692 for $c = 5$, and 2.759 for $c = 10$. Also, $\text{Re}(\omega)$ bifurcates at speeds $\bar{v}_{\text{bif}} < \bar{v}_{\text{crit}}$ for $c = 5$ and 10 , in contrast to when $c = 0$.

traveling strings. In this case the critical speed is 1 , matching the analytic solution in (Hagedorn and DasGupta, 2007). Figure 9(b), on the other hand, plots \bar{v} as a function of the scaled end tension and each curve corresponds to a different φ , similar to Fig. 4 for traveling Euler-Bernoulli beams. Although not as transparent as Fig. 9(a), we draw similar conclusions from Fig. 9(b). However, it is important to note that in contrast to beams (Fig. 4), the stability curves of strings in Fig. 9(b) are concave and they all converge to the critical speed of a horizontal string at high end-tensions.

The following example illustrates this discussion.

Example 2 The 0.5 mm steel cable mentioned in Example 1, when modeled as a traveling string, is stable for $T(L = 1\text{m}) = 1.75$ mN ($\mu_s = 1$) at travel speeds less than 1 m/s ($\bar{v} = 1$) when traveling horizontally ($\varphi = 0$), 0.8 m/s ($\bar{v} = 0.802$) when $\varphi = \pi/8$, 0.57 m/s ($\bar{v} = 0.582$) when $\varphi = \pi/4$ and 0.25 m/s ($\bar{v} = 0.254$) when traveling vertically ($\varphi = \pi/2$).

Thus, under the same end conditions, a traveling cable when modeled as string predicts a lesser critical speed than when it is modeled as an Euler-Bernoulli beam. This shows the stabilizing effect of bending rigidity EI in the beam. We further note that the difference between the critical speeds of Euler-Bernoulli beam and the string increases with the inclination φ . For this particular steel cable, the v_{crit} of the horizontally traveling Euler-Bernoulli beam (Example 1) is more than three times that of the horizontally traveling string (Example 2), while its almost ten when the cable is traveling vertically. Finally, higher end tension, for example $T(1\text{m}) = 7$ mN ($\mu = 2, \mu_s = 1$) or $T(1\text{m}) = 28$ mN ($\mu = 4, \mu_s = 1$), considerably reduces the difference in their respective critical speeds. However, any further increase in $T(L)$ doesn't reduce the difference much, and the $v_{\text{crit}}^{\text{EB beam}} > v_{\text{crit}}^{\text{String}}$

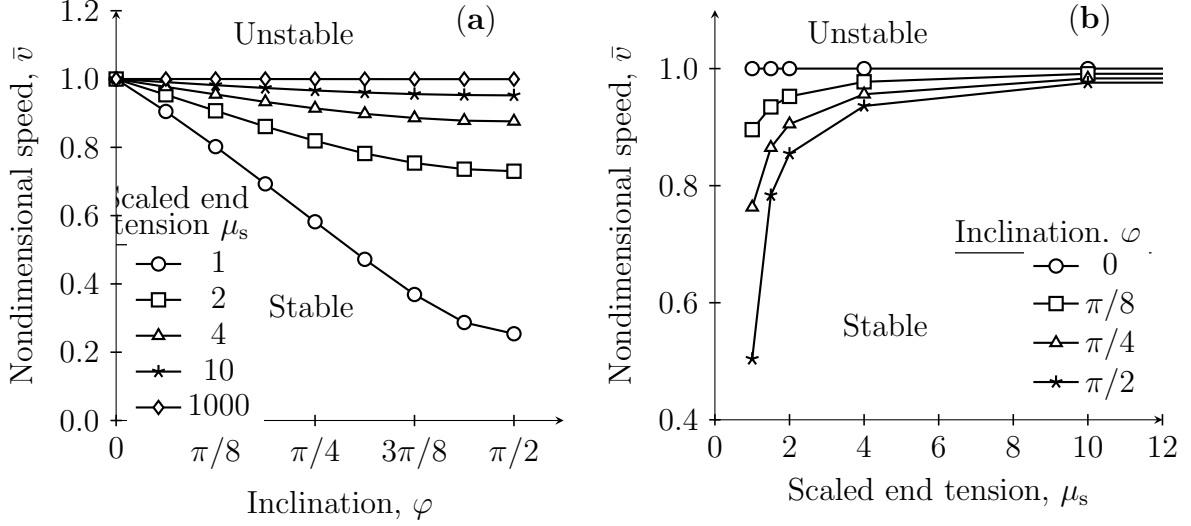


Figure 9: (a): Nondimensional speed \bar{v} of traveling strings as a function of their inclination φ for several choices of scaled end tension μ_s . (b): Nondimensional speed \bar{v} of traveling strings as a function of their scaled end tension μ_s for several values of inclination φ .

at all φ .

5 Energetics

Further insight into the system is provided by investigating the manner in which energy flows into and away from a traveling cable. This also has practical design implications. In this section we examine the flow of energy in traveling Euler-Bernoulli beams below and above the critical speed.

The total mechanical energy per unit length of the beam is

$$\bar{E}(\bar{x}, \bar{t}) = \bar{E}_K(\bar{x}, \bar{t}) + \bar{E}_P(\bar{x}, \bar{t}),$$

where the kinetic energy density

$$\bar{E}_K(\bar{x}, \bar{t}) = \frac{1}{2}(\bar{v}^2 + \dot{\bar{y}}^2)$$

and the potential energy density

$$\bar{E}_P(\bar{x}, \bar{t}) = \frac{1}{2}(\bar{\partial}_x^2 \bar{y})^2 + \frac{\bar{T}(\bar{x})}{2}(\bar{\partial}_x \bar{y})^2 + \varrho \bar{x} \sin \varphi.$$

The total rate of change of mechanical energy is

$$\dot{\bar{E}}(\bar{t}) = \int_0^1 \bar{\partial}_t \bar{E} + \bar{v} \bar{\partial}_x \bar{E} d\bar{x} = \left| \{ \bar{T}(\bar{x}) \bar{\partial}_x \bar{y} - \bar{\partial}_x^3 \bar{y} \} (\bar{v} \bar{\partial}_x \bar{y}) \right|_0^1 + \int_0^1 (\varrho \sin \varphi \bar{\partial}_x \bar{y}) (\bar{v} \bar{\partial}_x \bar{y}) d\bar{x}, \quad (14)$$

where the first term is the power supplied to the cable across the end supports by the action of the transverse component of tension and shear force. This term estimates the inflow and outflow of energy from the boundaries due to the presence of non-zero convective velocity $\bar{v} \bar{\partial}_x \bar{y}$ there; note that the local velocity $\bar{\partial}_t \bar{y}$ vanishes at the supports. The second term in (14) is the contribution of the cable's self-weight, due to its inclination, which vanishes for a horizontally traveling cable.

The time rate of change of energy (14) is zero in a non-translating ($\bar{v} = 0$) cable, but not if the cable is translating. In this the traveling cable exhibits a *non-conservative* behaviour. This behaviour, however, doesn't imply that the traveling cable is always unstable. Recall that through modal analysis (Sec.4.1) it was possible to identify a range of travel speeds and other system parameters for stable operations. Therefore, in the following, we study the stability of horizontally and vertically traveling cable by monitoring the evolution of the total mechanical energy and the transverse displacement of a material particle passing through the mid-span ($x = L/2$) of the cable.

Transverse displacement and the rate of change of energy

A standard explicit (Runge-Kutta) numerical time-integration of the state space equation (11) is performed to obtain the temporal coefficients $\mathbf{b}(t)$. The traveling cable is assumed to be released from a displaced configuration corresponding to its first mode. Accordingly, the initial conditions are: $\mathbf{b}(0) = [0.01, 0, 0, \dots]^T$ and $\dot{\mathbf{b}}(0) = [0, 0, 0, \dots]^T$. The transverse displacement at $\bar{x} = 0.5$ is then calculated from (10), and the rate of change of total energy $\dot{\bar{E}}$ is obtained from (14). Figures 10 and 11 show the evolution of transverse displacement and $\dot{\bar{E}}$ for a horizontally and vertically ($\varphi = \pi/2$) traveling Euler-Bernoulli beam, respectively. The results at sub-critical and super-critical operations are compared keeping the critical speed corresponding to $\mu = 1$ and $\varrho = 10$ from Fig. 4 as reference. The displacement \bar{y}_{sub} and rate of change of energy $\dot{\bar{E}}_{\text{sub}}$ correspond to operation at sub-critical speed $\bar{v}_{\text{sub}} < \bar{v}_{\text{crit}}$, while \bar{y}_{sup} and $\dot{\bar{E}}_{\text{sup}}$ are calculated at super-critical speed $\bar{v}_{\text{sup}} > \bar{v}_{\text{crit}}$.

The sub-critical $\dot{\bar{E}}_{\text{sub}}$ and \bar{y}_{sub} are oscillatory and bounded over an extended period of time (see Fig. 10). This is in agreement with Fig. 3, in which, at speeds lower than critical speed the real part of the first eigenvalue is zero. However, at super-critical speed \bar{v}_{sup} , both the energy rate and displacement amplitude show rapid growth. At this speed, as shown in Fig. 3, $\text{Re}(\omega_1^{\text{sup}})$ is positive and $\text{Im}(\omega_1^{\text{sup}})$ vanishes, so that the displacement \bar{y}_{sup} grows exponentially with time at the rate $\omega_1^{\text{sup}} = \text{Re}(\omega_1^{\text{sup}}) = 0.068$ as shown in the inset of Fig. 10. Also note that the growth is linear and small for a while before taking off exponentially. With further increase in speed this exponent becomes larger and the growth in amplitude is even faster. Gravity, as discussed previously, only worsens the stability, as shown in Fig. 11. Thus, in Fig. 11, the growth in amplitude for super-critical speed appears earlier and faster in time as compared to the horizontally traveling cable. We observe from the inset of Fig. 11, in contrast to the inset of Fig. 10, that during vertical travel the initial growth is fairly rapid, which causes the amplitude to shoot up before growing exponentially at the same rate $\omega_1^{\text{sup}} = 0.068$. From this we may infer that the instability in operation appears earlier in an inclined traveling cable than in a horizontal cable. Thus, the results of energetics and transient analysis support those found from modal analysis.

The super-critical energy rate $\dot{\bar{E}}_{\text{sup}}$ grows monotonically for a horizontally traveling cable (Fig. 10), whereas the growth is non-monotonous in case of vertically traveling cable (Fig. 11). This non-monotonous growth in the latter case is due to the second term in

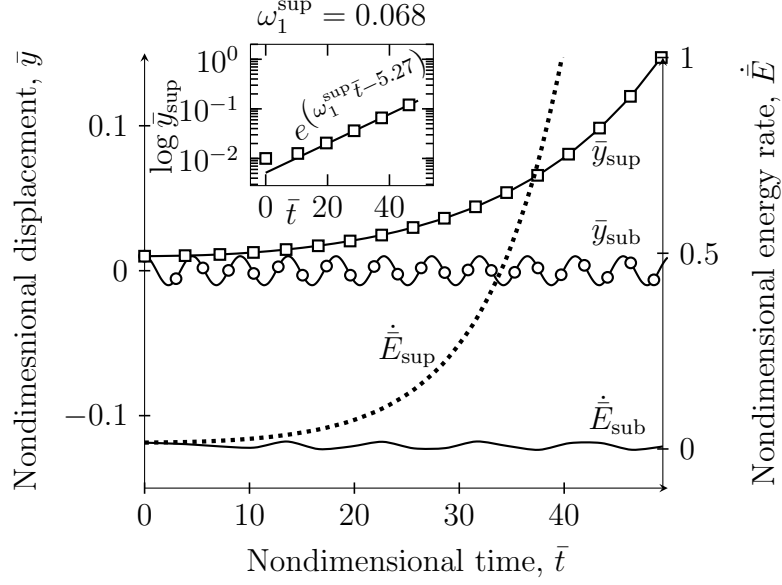


Figure 10: Temporal evolution of the transverse nondimensional displacement of the horizontally traveling cable at $\bar{x} = 0.5$ ($x = L/2$) and the rate of change of total mechanical energy (nondimensional). The sub-critical and super-critical nondimensional speeds are $\bar{v}_{\text{sub}} = 3.26$ and $\bar{v}_{\text{sup}} = 3.27$, respectively. The inset semi-log plot shows that \bar{y}_{sup} (\square) grows modestly for some period following which the growth is exponential (—) at a rate $\omega_1^{\text{sup}} = \text{Re}(\omega_1^{\text{sup}}) = 0.068$.

(14), which is a contribution of cable's weight that is absent during horizontal travel. Unlike the first term in (14), which is calculated only at the boundaries, the second term is obtained after integration over the cable's length. Therefore, at super-critical speed, the purely exponential growth of \bar{y}_{sup} causes $\dot{\bar{E}}_{\text{sup}}$ to grow non-linearly for both horizontally and vertically traveling cables, while the averaged quantity introduces oscillations in $\dot{\bar{E}}_{\text{sub}}$ for the vertically traveling cables.

6 Conclusions

In this paper, we studied the vibration analysis of a tensioned, heavy cable traveling inclined to gravity with a constant speed. The cable was modeled as a beam resisting tension, shear and bending. Modal analysis was performed for both the Rayleigh and the Euler-Bernoulli beam models. We identified the critical values of those parameters at which instability occurs; namely inclination, speed of travel, end-tension, slenderness ratio and bending rigidity. Stability curves, or boundaries, were obtained in the space of these parameters. The transient and energy analyses on the Euler-Bernoulli model were used to verify these boundaries. As a special case, highly flexible cables with zero bending rigidity were modeled as strings.

The instability in modal analysis was identified with the critical value of parameter at which the real part of the smallest eigenvalue first becomes positive. For the Euler-Bernoulli beam the critical speed \bar{v}_{crit} coincides with the speed \bar{v}_{bif} corresponding to the bifurcation of the real part of eigenvalue and simultaneous vanishing of the associated imaginary part. Physically, this phenomenon corresponds to exponential growing of the

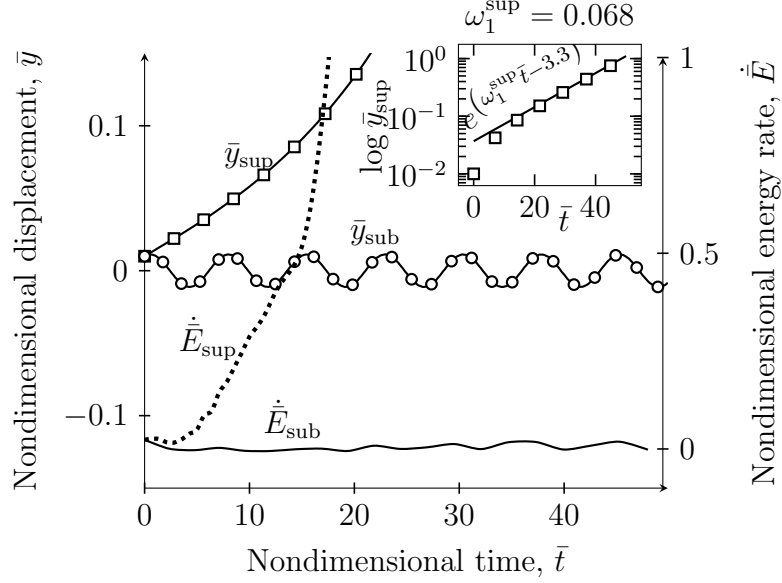


Figure 11: Temporal evolution of the transverse nondimensional displacement of the vertically traveling cable at $\bar{x} = 0.5$ ($x = L/2$) and the rate of change of total mechanical energy (nondimensional). The sub-critical and super-critical nondimensional speeds are $\bar{v}_{\text{sub}} = 2.37$ and $\bar{v}_{\text{sup}} = 2.38723$, respectively. The inset semi-log plot shows that \bar{y}_{sup} (\square) grows exponentially, at a rate $\omega_1^{\text{sup}} = \text{Re}(\omega_1^{\text{sup}}) = 0.068$, after a rapid initial rise in its amplitude.

amplitude of the displacement \bar{y}_{sup} at a rate $\omega_1^{\text{sup}} = \text{Re}(\omega_1^{\text{sup}})$, while the rate of energy influx also appears to rise. In contrast to Euler-Bernoulli beam, \bar{v}_{crit} and \bar{v}_{bif} are different for a Rayleigh beam.

Our observations are as follows. Firstly, the applied end-tension enhances the stability of a traveling cable system, while the action of gravity, due to the cable's inclination, lowers it. This is observed regardless of whether the traveling cable is modeled as a beam or as a string. Secondly, slenderness ratio improves the stability of the system. However, the effect of slenderness is more clearly observed when a traveling cable is modeled as a Rayleigh beam rather than an Euler-Bernoulli beam. When slenderness ratios are high both the models give close results. Thirdly, while an inclined traveling Rayleigh beam shows instability for all travel speeds, i.e. $\bar{v}_{\text{crit}} = 0$ and $\bar{v}_{\text{bif}} > \bar{v}_{\text{crit}}$, the effects of inclination on the stability of Euler-Bernoulli beam are negligible. However, the inherent instability of Rayleigh beam can be removed by inclusion of damping. When damping is included, $\bar{v}_{\text{bif}} < \bar{v}_{\text{crit}}$ and the Rayleigh beam undergoes underdamped oscillations at sub-bifurcation travel speeds. In Euler-Bernoulli beams the damping further enhances the stability. Lastly, the time rate of change of energy $\dot{\bar{E}}$ of the traveling cable is not constant, exhibiting a non-conservative behaviour. This behaviour doesn't necessarily imply instability at all speeds of travel. At sub-critical speeds, $\dot{\bar{E}}_{\text{sub}}$ is oscillatory and remains bounded for extended period of time. Whereas, at super-critical speeds $\dot{\bar{E}}_{\text{sup}}$ grows monotonically for horizontally traveling cables and non-monotonically for inclined traveling cables. Both $\dot{\bar{E}}_{\text{sup}}$ and \bar{y}_{sup} grow rapidly at higher inclinations, thus, confirming the destabilizing effect caused by the action of gravity.

A Convergence of solution

The converged values of critical speed for different inclinations are found by progressively increasing the number N of sine functions until the relative error between two successive computations becomes lower than 0.001%. For the horizontally traveling cable, the computed values of critical speed from beam and string models are compared with those obtained by employing Green's functions in (Wickert and Mote, 1990). Additionally, we solved (11) numerically utilizing 2-node Hermitian finite elements (FE). The converged solution from this procedure is in excellent agreement with that found through Galerkin projection with Fourier sine bases. Figure 12(a) plots the relative error

$$\varepsilon_{\text{crit}}^v = \left| 1 - \frac{v_{\text{crit}}^N}{v_{\text{crit}}^{\text{ref}}} \right| \cdot 100$$

in calculating the critical speed for an Euler-Bernoulli beam at different values of N . Similarly, Fig. 12(b) plots the relative error

$$\varepsilon_{\text{sub}}^\omega = \left| 1 - \frac{\omega_1^N}{\omega_1^{\text{ref}}} \right| \cdot 100$$

in calculation of the first eigenvalue at a sub-critical speed. For horizontally traveling beams the closed form results of (Wickert and Mote, 1990) are taken as reference. We conclude that both FE solution and Galerkin projection with Fourier sine bases are accurate when $N \geq 9$.

References

- Sack, R., 1954. "Transverse oscillations in travelling strings". *Brit. J. Appl. Phys.*, **5**(6), p. 224.
- Miranker, W. L., 1960. "The wave equation in a medium in motion". *IBM J. Res. Dev.*, **4**(1), pp. 36–42.
- Swope, R. D., and Ames, W. F., 1963. "Vibrations of a moving threadline". *J. Frankl. Inst.*, **275**(1), pp. 36–55.
- Mote, C., 1965. "A study of band saw vibrations". *J. Frankl. Inst.*, **279**(6), pp. 430–444.
- Mote, C., 1966. "On the nonlinear oscillation of an axially moving string". *J. Appl. Mech.*, **33**(2), pp. 463–464.
- Barakat, R., 1968. "Transverse vibrations of a moving thin rod". *J. Acoust. Soc. Am.*, **43**(3), pp. 533–539.
- Thurman, A., and Mote, C. D., 1969. "Free, periodic, nonlinear oscillation of an axially moving strip". *J. Appl. Mech.*, **36**(1), pp. 83–91.
- Rogge, T., 1972. "Equations of motion for flexible cables". *J. Aircraft*, **9**(11), pp. 799–800.
- Wickert, J., and Mote Jr, C., 1989. "On the energetics of axially moving continua". *J. Acoust. Soc. Am.*, **85**(3), pp. 1365–1368.
- Wickert, J., and Mote, C., 1990. "Classical vibration analysis of axially moving continua". *J. Appl. Mech.*, **57**(3), pp. 738–744.
- Wickert, J., 1992. "Non-linear vibration of a traveling tensioned beam". *Int. J. Nonlin. Mech.*, **27**(3), pp. 503–517.
- Ziegler, H., 2013. *Principles of structural stability*, Vol. 35. Birkhäuser.

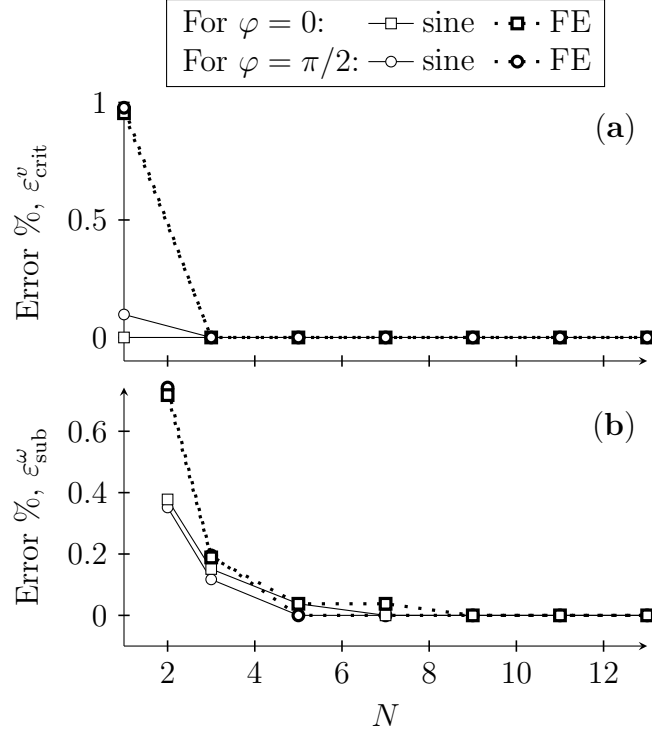


Figure 12: Plot (a) compares the errors in critical speed v_{crit}^N obtained from the N -term (Fourier) sine approximation and the N -element FE solution at various inclinations. In each case $\mu = 10$. For $\varphi = 0$ (horizontally traveling cable) the critical speed $v_{\text{crit}}^{\text{ref}} = 10.48$, as found by Wickert and Mote, 1990. For $\varphi = \pi/2$, the critical velocity calculated using $N = 399$ terms is taken as the reference. Plot (b) compares errors in the calculation of the first eigenvalue ω_1 at sub-critical speed $v_{\text{sub}}^{\text{ref}} = 5$.

- Alekseev, N. I., 1964. “On the equilibrium shape and tension of a flexible string acted upon by external forces that are functions of the orientation of the string in space”. *PMM*, **28**(5), pp. 1147–1150.
- Hagedorn, P., and DasGupta, A., 2007. *Vibrations and Waves in Continuous Mechanical Systems*. Wiley.
- Banichuk, N., Jeronen, J., Neittaanmäki, P., Saksa, T., and Tuovinen, T., 2013. *Mechanics of Moving Materials*. Solid Mechanics and Its Applications. Springer International Publishing.
- Meirovitch, L., and Hagedorn, P., 1994. “A new approach to the modelling of distributed non-self-adjoint systems”. *J. Sound Vib.*, **178**(2), pp. 227–241.